ADVANCED MATERIALS TECHNOLOGIES
www.advmattechnol.de

Aptamer-Capped Nanoporous Anodic Alumina for SARS-CoV-2 Spike Protein Detection

Isabel Caballos, María Nieves Aranda, Alba López-Palacios, Luis Pla, Sara Santiago-Felipe, Andy Hernández-Montoto, María Ángeles Tormo-Mas, Javier Pemán, María Dolores Gómez-Ruiz, Eva Calabuig, Beatriz Sánchez-Sendra, Clara Francés-Gómez, Ron Geller, Elena Aznar,* and Ramón Martínez-Máñez**

The COVID-19 pandemic, which began in 2019, has highlighted the importance of testing and tracking infected individuals as a means of mitigating the spread of the virus. In this context, the development of sensitive and rapid methods for the detection of SARS-CoV-2, the virus responsible for COVID-19, is crucial. Herein, a biosensor based on oligonucleotide-gated nanomaterials for the specific detection of SARS-CoV-2 spike protein is presented. The sensing system consists of a nanoporous anodic alumina disk loaded with the fluorescent indicator rhodamine B and capped with a DNA aptamer that selectively binds the SARS-CoV-2 spike protein. The system is initially evaluated using pseudotype virus systems based on vesicular stomatitis virus carrying different SARS-CoV-2 S-proteins on their surface. When the pseudotype virus is present, the cap of the solid is selectively removed, triggering the release of the dye from the pore voids to the medium. The nanodevice demonstrated its ability to detect pseudotype virus concentrations as low as $7.5 \cdot 10^3$ PFU mL. In addition, the nanodevice is tested on nasopharyngeal samples from individuals suspected of having COVID-19.

1. Introduction

Coronavirus disease 2019 (COVID-19) caused by SARS-CoV-2 coronavirus has rapidly spread all over the world resulting in a global pandemic, counting with more than 613 million SARS-CoV-2-infected confirmed cases and more than 6 500 000 reported deaths worldwide until September 2022.[1] The main symptoms caused by this positive-stranded RNA virus are similar to acute respiratory infection, like cough, fever, loss of taste and smell and difficulty breathing. The most exposed population are elderly people, adolescents, infants, and people with the compromized immune system.[2] The high capacity of dissemination of the virus requires to identify the presence of SARS-CoV-2 in an accurate and rapid way. This is desirable not only for the identification

I. Caballos, M. N. Aranda, A. López-Palacios, L. Pla, S. Santiago-Felipe, A. Hernández-Montoto, E. Aznar, R. Martínez-Máñez
Instituto Interuniversitario de Investigación de Reconocimiento Molecular y Desarrollo Tecnológico
Universitat Politècnica de València
Universitat de València
Camino de Vera s/n, 46022, Valencia, Spain
E-mail: elazgi@upvnet.upv.es; rmaez@qim.upv.es

I. Caballos, M. N. Aranda, A. López-Palacios, L. Pla, S. Santiago-Felipe, A. Hernández-Montoto, E. Aznar, R. Martínez-Máñez
Unidad Mixta de Investigación en Nanomedicina y Sensores.
Universitat Politècnica de València
Instituto de Investigación Sanitaria La Fe (IISLAFE)
Avenida Fernando Abril Martorell
Valencia 106, 46026, Spain

The ORCID identification number(s) for the author(s) of this article can be found under https://doi.org/10.1002/admt.202201913.

DOI: 10.1002/admt.202201913

I. Caballos, M. N. Aranda, A. López-Palacios, L. Pla, S. Santiago-Felipe, A. Hernández-Montoto, E. Aznar, R. Martínez-Máñez
CIBER de Bioingeniería, Biomateriales y Nanomedicina (CIBER-BBN)
Instituto de Salud Carlos III
Valencia, Spain

M. Á. Tormo-Mas, J. Pemán, M. D. Gómez-Ruiz, E. Calabuig
Grupo Infección Grave
Hospital Universitari i Politècnic La Fe
Instituto de Investigación Sanitaria La Fe (IISLAFE)
Avenida Fernando Abril Martorell
Valencia 106, 46026, Spain
E-mail: tormo_man@iislafe.es

J. Pemán, M. D. Gómez-Ruiz
Servicio de Microbiología
Grupo Infección Grave
Hospital Politècnic i Universitari La Fe. Instituto de Investigación Sanitaria La Fe (IISLAFE)
Avenida Fernando Abril Martorell
Valencia 106, 46026, Spain

E. Calabuig
Unidad de Enfermedades Infecciosas
Hospital Politècnic i Universitari La Fe. Instituto de Investigación Sanitaria La Fe (IISLAFE)
Avenida Fernando Abril Martorell
Valencia 106, 46026, Spain

of infected patients but also for the detection of asymptomatic and presymptomatic people.[3,4] To manage with this global concern, it is necessary to provide the society with a wide collection of different systems that could afford the massive demand of tests releasing the appropriate information. Given the global impact of COVID-19, there is a need for the development of highly accurate approaches for the rapid identification of biomarkers of SARS-CoV-2 infection in patient samples, including ribonucleic acid (RNA), antigens, antibodies, or directly the whole virus.

The real-time quantitative reverse transcription polymerase chain reaction (RT-qPCR) is currently the standard test to detect this virus. This approach often requires laboratory facilities, trained personnel, expensive instrumentation, and the assay takes hours to provide a result. In addition, RT-qPCR is not always available in underdeveloped and developing countries where the vast population lives in the backcountry.[5] Besides, considering the increasing infection rate, PCR methods are not sufficient to cover the current testing demand. Another commonly used approach is serological testing, which is not recommended when the viral load is very low, for example in the early stages of the infection, since the serological antibodies will not be present until a couple of weeks after the initial viral infection.[6] In contrast, antigen detection systems, which rely on the identification of a specific immunogenic component of a pathogen, typically a polysaccharide molecule or a protein, as a means of detecting the presence of the pathogen, have gained general approval thanks to their detection speed, simplicity, low cost, and accuracy. The drawback of the technique is that current sensitivity levels are still poor leading to a high variability and low performance depending on the manufactured brand. Antigen detection systems are usually used as screening tests for example in large groups or as a previous exploratory test before the realization of a more accurate molecular and/or serologic assay.[7] Based on the above, it can be concluded that there is still room to develop a test that combines the sensitivity and accuracy of the PCR methods and the low-priced and rapid antigen detection procedures in order to deal with the spread of the virus and control potential new outbreaks.[8,9]

Recently, biosensors targeting pathogens or infection biomarkers based on nanotechnology have become more and more popular owing to their capacity to supply accurate, sensitive, and reliable results, revolutionizing the healthcare industry. Multiple reported designs have demonstrated that it is possible to obtain numerous benefits from the combination of the usefulness and versatility of nanomaterials with the recognition properties of sensitive and highly selective biomolecules.[10] On this point, some new approaches have been extensively applied in the development of sensing systems with a huge variety of applications, which enhanced the sensitivity of already available detection systems. Among the great variety of nanomaterials available to develop sensitive biosensors, nanoporous anodic alumina (NAA) offers easy modification of the surface, high loading capacity and its production can be easily arranged by standard production techniques that are cost-competitive.[11] In the last years, NAA have been used to develop gated nanomaterials for biosensing applications. In those systems, only the target pathogen o biomolecule induces the release of the entrapped reporter.[12–14] For example, we have previously reported oligonucleotide-capped mesoporous supports for the detection of *Staphylococcus aureus*[15] and *Candida auris* DNA in blood culture specimens from infected individuals, bringing gated materials into clinical settings and showing their enormous potential.[16]

Among the possible gating mechanism that can be implemented on porous supports to configure a functional sensory material, aptamers have demonstrated excellent performances. Aptamers consist of small peptide molecules or more commonly oligonucleotide sequences having high specific binding affinity for their target molecules leading a precise and accurate detection. By using the appropriate linkers and coupling agents, aptamers can be easily adapted to any specific design.[17,18] As a consequence, such small proteins or oligonucleotides have been widely used to develop sensing systems known as aptasensors. The purity, high stability, and reversibility of these devices under harsh environmental conditions, combined with the availability of target-specific linkers, make them ideal for novel diagnostics.[19]

Biosensors based on aptamers have been demonstrated to be a highly effective analytical tool for the rapid diagnosis of infections, with high sensitivity and specificity. In the case of SARS-CoV-2 detection, Zhang et al.[8] developed a system for the detection of SARS-CoV-2 that utilizes aptamer probes that bind to a specific protein target, bringing together a ligation DNA region in close proximity and initiating ligation-dependent qPCR amplification. Another example has been reported by Sandall et al.[20] who described the development of a system based on the use of an intrinsic silicon thin film transistor functionalized with aptamers that specifically bind to the SARS-CoV-2 spike protein. Also, several examples using nanomaterials and aptamers to recognize SARS-CoV-2 targets have been described. For example, Tabrizi and coworkers developed a photoelectrochemical aptasensor based on graphitic carbon nitride combined with CdS quantum dots and chitosan to obtain a nanocomposite which is further functionalized with a RBD spike domain sensitive aptamer.[21] In another approach, Ray et al. took advantage of distance-dependent nanoparticle surface energy transfer phenomena to detect spike protein by fluorescence quenching induced thanks to aptamer-functionalized gold nanostars.[22]

Taking into account literature reports, it can be envisioned the potential of combining the excellent performance of gated materials and aptamers to configure a functional nanomaterial for SARS-COV-2 infection biomarkers recognition. Based on this premise, herein we report a method for highly ultrasensitive and specific detection of SARS-CoV-2-associated antigens, in particular the spike protein receptor-binding domain, based on aptamer-capped gated NAA. In our design, NAA supports were first loaded by diffusion with the fluorescent reporter dye rhodamine B, followed by the capping with an aptamer that specifically binds with the spike protein of SARS-CoV-2 virus. As a capping system the aptamer described by Yang et al.[23] was selected due to its suitable properties like the absence of

B. Sánchez-Sendra, C. Francés-Gómez, R. Geller
I^{2}SysBio
Universidad de Valencia-CSIC. Calle del Catedrático Agustín Escardino 9
Paterna 46980, Spain

secondary structures formation, molecular weight, and target affinity. Once the system is arranged, the capping aptamer inhibits dye release blocking the pores. Only in the presence of SARS-CoV-2 spike protein, the capping aptamer is displaced (thanks to the specific hybridization between aptamer and protein), uncapping the pores and allowing dye release. The capped sensing aptasensor was also tested using pseudotype virus systems based on vesicular stomatitis virus (**VSV**) carrying different SARS-CoV-2 S-proteins on the surface. Finally, the system has been tested in patient samples. The prepared materials are found to respond rapidly, allowing accurate detection in buffer and nasopharyngeal samples in just one hour.

2. Results and Discussion

2.1. Synthesis and Characterization of Gated NAA

In our proposed system, NAA pores were loaded with rhodamine B fluorescent reporter and the surface was chemically modified by attaching (3-triethoxysilyl)propylisocyanate, to give support **S1**. Then, two oligonucleotides NH_2-$(CH_2)_6$-5′-AAA AAA CCC CCC-3′ (**O1**) and 5′-TTT TTG GGG GGC AGC ACC GAC CTT GTG CTT TGG GAG TGC TGG TCC AAG GGC GTT AAT GGA CAG GGG GGT TTT T-3′ (**O2**) were used to obtain a capped nanomaterial through strong covalent and hydrogen bonding interactions. First, **O1**, which has been engineered to identify and bind with the sequence 3′-TTT TGG GGG G-5′ included in **O2**, was covalently anchored by the formation of urea bonds with the isocyanate moieties present in **S1** to obtain support **S2**. In the second step, **O2**, which contains the specific aptamer sequence to recognize SARS-CoV-2 spike protein (i.e. 5′-CAG CAC CGA CCT TGT GCT TTG GGA GTG CTG GTC CAA GGG CGT TAA TGG ACA-3′), was employed in a concentration of 8 µM to hybridize with **O1** and block the pores of **S2**, obtaining the final sensing gated nanomaterial **S3** (see Experimental Section for further details). This aptamer was selected from a pool of three aptamers described by Yang et al.[23] which were able to recognize independently the SARS-CoV-2 spike protein or the nucleocapsid protein. The three candidates were tested at concentrations ranging 5.6-12 µM and finally, aptamer **O2** was selected due to its better capping ability and controlled release performance. Aptamer **O2** holds a K_d value (equilibrium dissociation constant) of 5.8 nM.[23] The **O1–O2** complex made of double-stranded DNA on the outer surface of the inorganic scaffold is anticipated to be large enough to block pores and prevent dye delivery. In contrast, in the presence of the target spike SARS-CoV-2, the capping aptamer will recognize the SARS-CoV-2 spike protein. This would lead to a displacement of the **O2** sequence form the surface of the functional material, resulting in cargo release (**Figure 1**).

Raw NAA material, **S1**, **S2**, and **S3** were characterized by EDX and FESEM techniques. In commercially available NAA supports, anodic aluminum oxide films are grown on aluminum layers with pore densities of 9×10^{11} cm^{-2}. There is a funnel-like shape to the pore entrance which gradually shrinks starting at a size of 20–30 nm at the top and decreasing to 5 nm at the bottom. The pores are as long as 10 µm. As the material was cut into disks of 2 mm in diameter. The appearance of the initial material was a silver small disk while once loaded with rhodamine B it becomes of an intense pink color (from **S1** to **S3**) that does not fade with the posterior treatments. Pictures of the raw NAA material and final **S3** support is shown in the insets of **Figure 2**. Representative FESEM images of the starting NAA scaffold showed the porous structure described above (Figure 2a). Besides, images of **S3** evidenced the presence of a dense capping layer on the top of the pores (Figure 2b) confirming a compact pore capping. We have also verified through FESEM microscopy that when the SARS-CoV-2 spike protein is present, most of the part of the superficial organic layer detaches compared to the control (see Supporting Information).

X-ray energy-dispersive spectroscopy was used to analyze the organic content of **S2** and **S3** (Table 1). **S1** was found to contain a high carbon content (C/Al 4.771), as expected due to the large loading capacity of the NAA material. As a result of the experimental conditions for **O1** attachment, solid **S2** has a lower carbon content than solid **S1**, indicating partial cargo release (C/Al 0.353). Finally, solid **S3** also maintained a similar organic matter content. Likewise, it was confirmed in the final material a higher P/Al and N/Al content from the capping oligonucleotide.

Maximum amount of rhodamine B that can be released from the final material to the solution was also quantified by extraction experiments. As a result, a deliverable rhodamine B content was calculated to be ca. 0.33 µg mL^{-1}.

2.2. Release Assays

To examine the mechanism by which the material can be opened, the controlled release of the material in the solution was studied in the presence and absence of purified SARS-CoV-2 spike protein, which includes the receptor-binding domain that is targeted by the capping aptamer. To conduct this study, a hybridization buffer was used to submerge two independent gated supports of the **S3** solid. One support was then treated with 100 µL of purified SARS-CoV-2 spike protein (1 ng $µL^{-1}$), while the other was treated with 100 µL of TRIS buffer. At predetermined intervals, the fluorescence of the supernatant solution was measured to quantify the release of dye from the pores to the aqueous phase. The release profile of rhodamine B from the **S3** solid in the absence and presence of SARS-CoV-2 spike protein is shown in **Figure 3**a. When the **S3** solid is placed in a hybridization buffer alone, it releases a very small amount of dye (less than 10% of the maximum dye release), indicating tightly closed pores (Figure 3a, curve 1). In contrast, when the **S3** solid is placed in a solution containing SARS-CoV-2 spike protein, a significantly larger amount of rhodamine B is released (10-fold increase at 60 min, Figure 3a, curve 2).

In the next step, we validated the system using a model closer to clinical samples, demonstrating that the system can recognize a complete virus that expresses the target protein of SARS-CoV-2 on its surface. Research using pathogens classified as high biosafety levels, such as SARS-CoV-2, is complicated by the inherent difficulty of working under biosafety level 3 conditions. Hence, model systems are often preferred for many applications. Pseudotype virus systems provide such

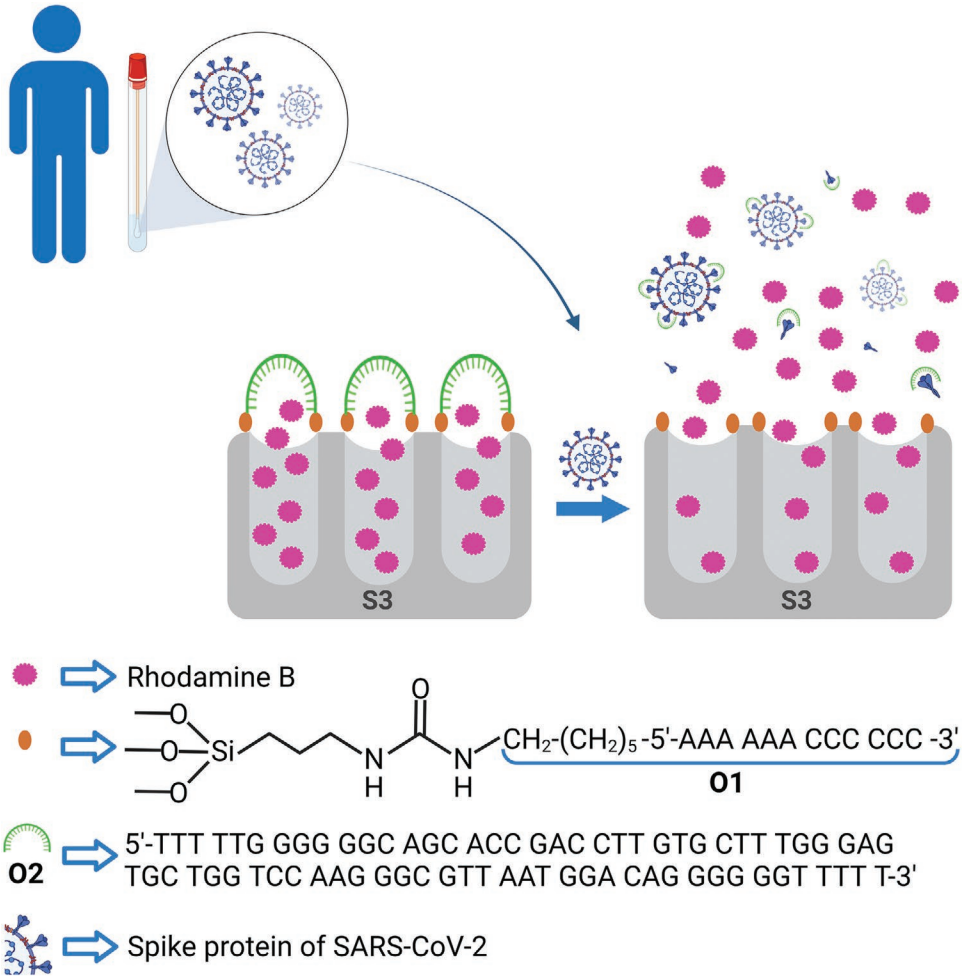

Figure 1. Scheme of the gated NAA material **S3** selectiveness for the recognition of SARS-CoV-2 spike protein. In the absence of the virus protein, pores are blocked while the presence of SARS-CoV-2 S protein induced aptamer displacement and delivery of the entrapped dye.

models. These are based on the use of a low biosafety level virus in which the viral envelope protein is deleted from the genome and replaced with that of a pathogenic virus, either by supplying it in trans or by encoding it within the viral genome. These systems have proved valuable for assaying entry mechanisms of diverse viruses, evaluation of neutralizing antibody levels, and discovery of antivirals, and as vaccines.[24] Moreover, as the pseudotype virus encodes a functional entry glycoprotein of a virus of interest, these can be used to safely and rapidly evaluate detection systems.

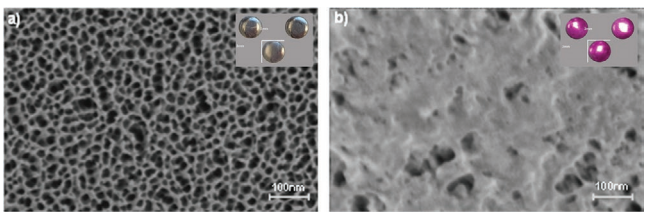

Figure 2. a) FESEM representative images of NAA support and b) gated solid **S3**. Insets feature photographs of the corresponding solids.

Based on the above, to simulate the presence of the virus in the sample we used a pseudotype virus system as a model system based on vesicular stomatitis virus (**VSV**) carrying different SARS-CoV-2 S-proteins on the surface (**VSV-S**). These **VSV** pseudotype viruses have been shown to enter cells in an analogous manner to SARS-CoV-2 but facilitate the evaluation of the system.[25] We employed both a replication-competent **VSV** encoding the Wuhan spike protein in place of its glycoprotein G (**VSV-S**), which grows to high titer, and replication-incompetent **VSV** where the spike protein from different variants was supplied in trans (see Experimental Section for further details). The viruses were named depending on the SARS-CoV-2 variant genome they were carrying as **VSV-Alpha**, **VSV-Beta**, **VSV-Gamma**, and **VSV-Delta**.

The behavior of two independent **S3** materials in hybridization buffer were studied in the presence of 100 µL of **VSV-S** pseudotype or **VSV** (without S-protein) and the amount of rhodamine B released to the solution was recorded by recording the fluorescence at different times at 575 nm (λ_{exc} = 555 nm) (Figure 3b). It was observed that SARS-CoV-2 spike protein (purified or attached to the pseudotyped virus) uncapped the pores and induced cargo delivery as represented in Figure 3.

Table 1. The relation of atomic elements in the different prepared solids.

	C/Al	N/Al	P/Al
S0	0.16 ± 0.00	–	–
S1	4.77 ± 0.10	0.74 ± 0.02	–
S2	0.35 ± 0.00	0.05 ± 0.00	0.00 ± 0.00
S3	0.35 ± 0.01	0.06 ± 0.00	0.01 ± 0.01

2.3. Sensitivity and Specificity Studies

To determine the sensitivity of the proposed method, experiments were conducted using **S3** at various concentrations of VSV-S and the resulting responses were analyzed. Eleven independent **S3** supports were immersed in hybridization buffer, and 100 µL aliquots of serial dilutions of the virus suspension were added to each material, resulting in final concentrations ranging from between 10^3 and 5×10^5 PFU mL^{-1} per milliliter (PFU mL^{-1}). After a 60 min incubation period, the total amount of rhodamine B released into the aqueous phase was quantified using fluorescence measurements. The results indicated a linear relationship between the concentration of VSV-S and the amount of dye released (**Figure 4**). Moreover, the limit of detection (LOD) of our system was calculated graphically from the intersection of the line of the points that present a base fluorescence with the line with a positive slope (Figure 4). The point in the x-axis on which this intersection point falls is the LOD that corresponds to 7.5×10^3 PFU mL^{-1}. Despite not being optimized for commercial purposes, instrumental SARS-CoV-2 detection techniques usually report LODs in the same range (Table S1, Supporting Information). However, when compared to current methods based on molecular techniques such as DNA amplification or sequencing, our biosensor based on oligonucleotide-capped nanoporous anodic alumina displays certain advantages: i) both the cargo and capping DNA sequences are highly tunable; ii) compared to other techniques, the cost of preparation and testing is significantly lower; iii) the equipment needed is simple, widely available, and cost-effective for most laboratories, and iv) it is faster, more straightforward, and does not require DNA extraction or amplification as part of the analysis process. Overall, our assay might provide a viable alternative to detect SARS-CoV-2 in a fast and precise manner.[26,27]

In order to further evaluate the selectivity of the **S3** biosensor for the detection of the SARS-CoV-2 spike protein, the response of **S3** was evaluated in the presence of 100 µL of purified spike protein (1 ng mL^{-1}) and eight different drugs in 900 µL of hybridization buffer (**Figure 5**). These drugs are commonly found in samples since they are commonly prescribed for the treatment of common illnesses or chronic diseases. As shown, the presence of the SARS-CoV-2 spike protein (or mixtures of SARS-CoV-2 spike protein and drug) was the only condition that resulted in a significant release of rhodamine B, while the presence of the drugs alone resulted in minimal uncapping and cargo delivery. This suggests that **S3** exhibits a highly selective response to the presence of the SARS-CoV-2 spike protein.

2.4. Detection of VSV-S in Nasopharyngeal Fluid and Inoculated Clinical Samples

Furthermore, the stability of the system was assessed by examining the behavior of **S3** in the presence of 100 µL of 2.5×10^5 PFU mL^{-1} of **VSV-S** was evaluated in 900 µL of a clinically relevant media, as it is a nasopharyngeal fluid obtained from four different healthy patients with the use of a collection swab in 5 mL of hybridization buffer (TRIS). As shown in **Figure 6**, the presence of **VSV-S** in this competitive medium also resulted in the selective displacement of the aptamer, pore uncapping, and dye release. A comparison of the residual release in nasopharyngeal fluid and buffer revealed a higher residual release in the former. Nevertheless, the fluorescence measurement in the presence of the virus was comparable to that observed in TRIS buffer. In addition, it is necessary to highlight how the nasopharyngeal fluid increases the fluorescence in the same rate for all samples (which have been collected from different patients).

In a further attempt, a small analytical assay was performed. Taking into account the usual SARS-CoV-2 concentration in nasopharyngeal samples (an average of 7×10^6 PFU mL^{-1} per sample until the fifth day of infection and a maximum of 7.11×10^8 copies per swab[28]), aliquots of negative nasopharyngeal samples were inoculated with different amounts of the pseudotyped virus **VSV-S** (5×10^3 to 4×10^4 PFU mL^{-1}) to

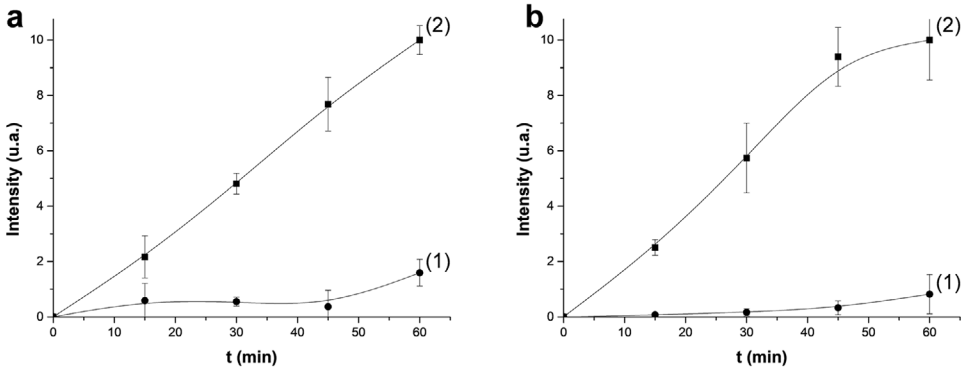

Figure 3. Time-dependent release of Rhodamine B from the pores of material **S3** in TRIS buffer (pH 7.5). Plot a) indicates dye release in the lack of any stimulus (1) and in presence of target purified spike protein at a concentration of 1 ng µL^{-1} (2). Plot b) illustrates cargo delivery in the presence of **VSV-S** (2.5×10^4 PFU mL^{-1}) (2) and in presence of **VSV** without any spike on its surface (2.5×10^4 PFU mL^{-1}) (1).

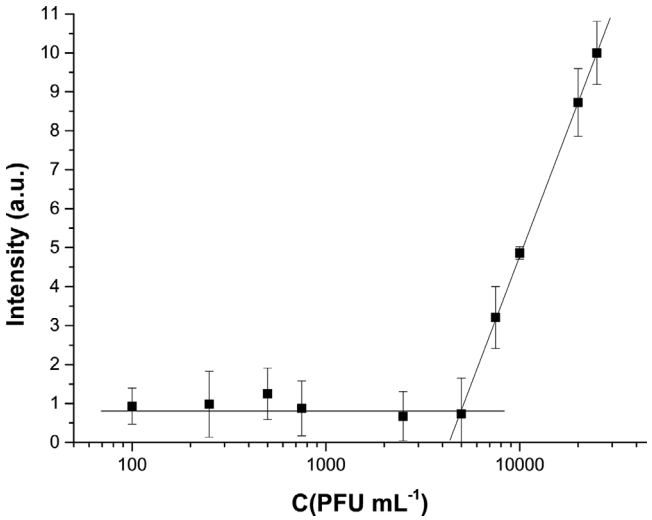

Figure 4. The release of dye from the **S3** solid in the presence of varying concentrations of VSV-S in TRIS buffer.

emulate SARS-CoV-2 infected samples. Subsequently, 100 µL aliquots of each sample were combined with a microtube containing the **S3** support and 900 µL of hybridization buffer. The release of rhodamine B from the pores was measured at a wavelength of 575 nm (excitation wavelength of 555 nm) after 60 min of incubation at 25 °C. Experimental points (**Figure 7**) show that the obtained signal is proportional to the concentration of **VSV-S**. The possibility of obtaining an approximation of the virus concentration in the samples is of interest in a clinical context, as it might allow differentiating patients with a high viral load and who may need a different treatment than others with a lower load. Additionally, preliminary investigations of the stability of the aptamer-gated nanomaterials have demonstrated that they can be stored for up to 8 weeks without any loss of performance.[29]

2.5. Study of the System Behavior with Different S Proteins from Different SARS-CoV-2 Variants of Concern

In a step forward, the response of **S3** to S protein from different SARS-CoV-2 variants of concern were studied using pseudotyped **VSV** carrying the different S protein variants Alpha, Beta, Gamma, and Delta (i.e. **VSV-Alpha**, **VSV-Beta**, **VSV-Gamma**, and **VSV-Delta**), which are the most spread in European countries until December 2021. In each experiment, **S3** was submerged in a nasopharyngeal sample doped with the pseudotyped virus carrying a spike protein with the corresponding genome of the variant of concern (**VSV-Alpha**, **VSV-Beta**, **VSV-Gamma**, and **VSV-Delta**). Released rhodamine B after 60 min was measured by fluorescence as in previous experiments. As can be appreciated in **Figure 8**, **S3** responds to all studied variants, giving hope to the detection of new coming variants of the virus using **S3**.

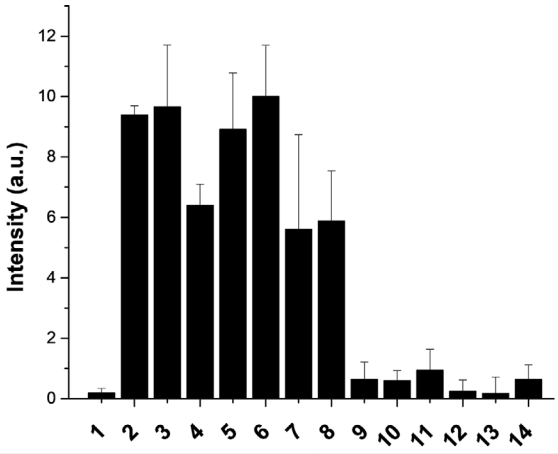

1	Blank	8	SP + Tiotropium 0.5 mg mL^{-1}
2	Spike protein (SP)	9	Salbutamol 0.1 mg mL^{-1}
3	SP + Salbutamol 0.1 mg mL^{-1}	10	Acetaminophen 0.1 mg mL^{-1}
4	SP + Acetaminophen 0.1 mg mL^{-1}	11	Acetylsalicylic acid 0.05 mg mL^{-1}
5	SP + Acetylsalicylic acid 0.05 mg mL^{-1}	12	Enoxaparin 0.1 mg mL^{-1}
6	SP + Enoxaparin 0.1 mg mL^{-1}	13	Levotyroxine 0.025 mg mL^{-1}
7	SP + Levotyroxine 0.025 mg mL^{-1}	14	Tiotropium 0.5 mg mL^{-1}

Figure 5. Media fluorescence intensity in the presence of drug interferents alone or in combination with the viral spike protein (1 ng µL^{-1}) in TRIS buffer after 60 min.

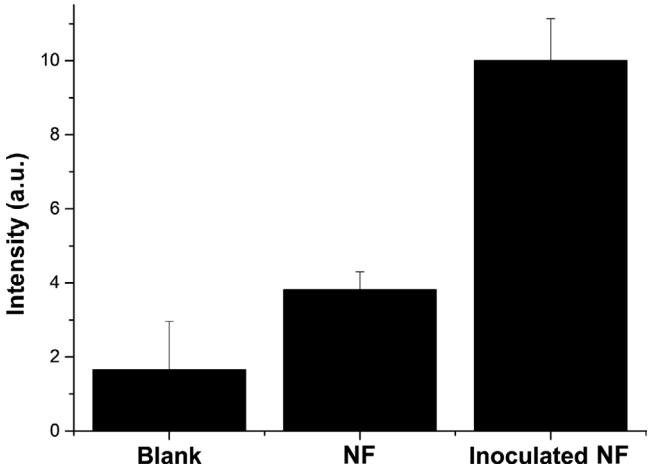

Figure 6. Delivery of rhodamine B from material **S3** in TRIS (Blank) in the presence of the stimulus, in nasopharyngeal fluid (**NF**) obtained from different patients and nasopharyngeal fluid inoculated with **VSV-S** (concentration: $2.5{\cdot}10^4$ PFU mL^{-1}) after 60 min.

2.6. Device Testing in Presence of Infected and Non-Infected Real Samples

Detecting the SARS-CoV-2 virus directly in clinical samples is crucial to apply the **S3** probe in clinical practice. Thus, the performance of the sensing materials to detect Spike protein from the infected patient sample were studied. The ongoing reference method for SARS-CoV-2 detection in most health centers is based on RT-qPCR which requires at least two hours until the results are obtained, with complex equipment, and trained personnel. In the present work, SARS-CoV-2 positive and negative clinical nasopharyngeal samples from Hospital Universitari i Politècnic La Fe were studied. The samples were analyzed by RT-qPCR and using **S3** (see Experimental Section for details). A total of 54 patients (59.3% men) were enrolled in the study; of them, 26 patients were diagnosed with COVID-19 pneumonia

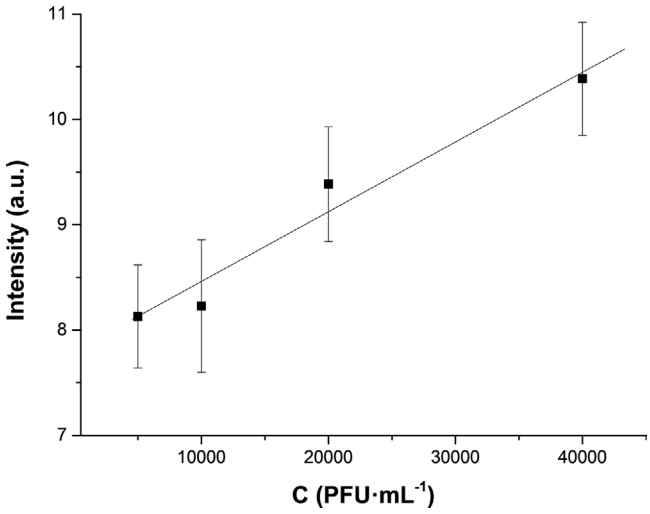

Figure 7. Rhodamine B release from pores of solid **S3** in the presence of increasing amounts of **VSV-S** (PFU mL^{-1}) in a clinical sample.

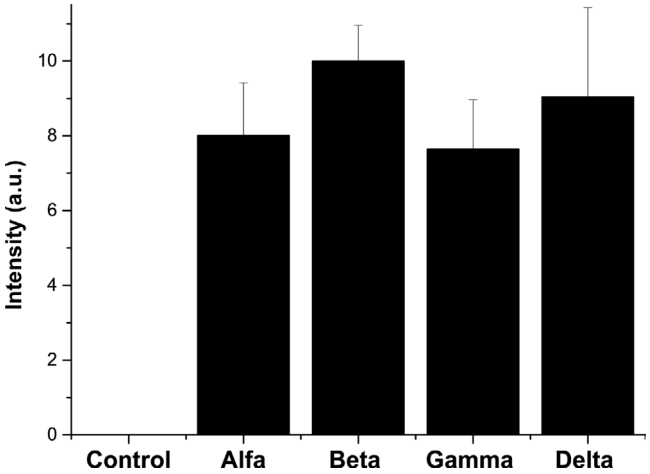

Figure 8. Media fluorescence intensity of rhodamine B in presence of **VSV-Alpha**, **VSV-Beta**, **VSV-Gamma,** and **VSV-Delta**. (2.5×10^4 PFU mL^{-1}). Control represents the delivery in the nasopharyngeal sample without the stimulus after 60 min from the beginning of the experiment. Control value was subtracted from all the raw values of each represented group. Then, the remaining values were relativized to a scale of 0–10, with being 10 the highest intensity fluorescence value and 0 being the lowest.

and 28, used as a negative control, were hospitalized for other reasons. The patient's characteristics are displayed in **Table 2**.

The samples were analyzed in duplicate using the gated material **S3** by immersing individual **S3** supports in 995 µL of TRIS and adding 5 µL of a nasopharyngeal sample (0.5%) to each one. The Fluorescence of released rhodamine B after 60 min was measured as in previous experiments. **Figure 9** shows how in general delivery of the dye from **S3** in the control samples (red dots) are lower than in positive samples (black dots), suggesting that **S3** is a suitable probe for SARS-CoV-2 detection.

Additionally, a final validation experiment was conducted using positive samples from patients infected with other viruses of the *coronaviridae* family such as HKU1, OC43, NL63, and 229E. Detection experiments were performed by duplicate using the gated final material. As in previous experiments, individual supports were immersed in 995 µL TRIS, and 5 µL of the samples were added in each respectively. Rhodamine B release was measured after 60 min showing the results represented in **Figure 10**. A selective response to SARS-COV-2 is observed.

3. Conclusion

Rapid and accurate detection of SARS-CoV-2 infections is crucial for preventing new outbreaks and ensuring appropriate treatment. Therefore, the development of new approaches for the simple and rapid identification of this virus is essential in clinical practice. As demonstrated in this study, nanoporous materials can be combined with aptamers to create a useful fluorescence-based biosensor for the detection of the SARS-CoV-2 spike protein in a competitive environment. The nanoporous anodic alumina (NAA) scaffold constitutes the biosensor, this support has been loaded with rhodamine B and capped with an aptamer specific to the SARS-CoV-2 spike protein. Upon

Table 2. Description of the patients from where the nasopharyngeal samples were obtained.

No. patients	Age range (years)	Gender M/F	Main Underlying diseases (%)					
			HBP[a)]	DM-II[b)]	Dyslipidemia	Hearth failure	Obesity	Hypothyroidism
COVID-19 ($n = 26$)	20–89	15/11	30.8	19.2	23.1	3.8	38.5	7.7
Control (n = 28)	27–98	17/11	50.0	48.2	50.0	14.3	3.6	10.7
Total ($n = 54$)	20–98	32/22	40.7	31.5	37.0	9.3	20.4	9.3

[a)]HBP (high blood pressure); [b)]DM-II (type II diabetes mellitus).

exposure to the spike protein or SARS-CoV-2 pseudotypes, the capping aptamer is displaced, the pores open, and the fluorophore is released. The biosensor exhibits a limit of detection of 7.5×10^3 PFU mL^{-1} in TRIS buffer and 2×10^4 PFU mL^{-1} in nasopharyngeal samples collected in TRIS media, which is comparable to the performance of other state-of-the-art SARS-CoV-2 detection systems. In addition, the biosensor demonstrates high selectivity for the SARS-CoV-2 spike protein and is not affected by other interfering substances. The proposed method was successfully applied to the identification of SARS-CoV-2 virus pseudotypes in artificially inoculated clinical samples and nasopharyngeal samples from COVID-19 patients. It is efficient in terms of sensitivity and predictive values and is fast, simple, and portable. It can also be easily modified by incorporating different reporters and capping sequences. This approach to sensing may also provide inspiration for the development of new simple tests for point-of-care pathogen testing.

4. Experimental Section

General Techniques: Field Emission Scanning Electron Microscopy (FESEM) and was performed using a ZEISS Ultra 55 microscope. Energy Dispersive X-ray spectroscopy (EDX) analysis was obtained with the same equipment. Fluorescence spectroscopy measurements were performed using a BioTek Synergy H1 microplate reader.

Reactives and Reagents: TRIS(hydroxymethyl)aminomethane (TRIS), (3-triethoxysilyl)propylisocyanate, rhodamine B, acetonitrile, and triethylamine (TEA) were provided by Sigma-Aldrich Química (Madrid, Spain). Nanoporous anodic alumina supports were purchased from InRedox® (CO, USA). Oligonucleotides were obtained from Integrated DNA Technologies, Inc. (IA, USA) and used without further purification.

Oligonucleotides Design: The aptamer sequence employed in this research was sourced from literature (refer to reference[23] for further details). It was obtained from IDT through Danaher Corporation located in Leuven, Belgium. The specific sequence selected to cap the pores was **O1**: 5′-AAA AAA CCC CCC-3′; **O2**: 5′-TTT TTG GGG GGC AGC ACC GAC CTT GTG CTT TGG GAG TGC TGG TCC AAG GGC GTT AAT GGA CAG GGG GGT TTT T-3′.

Synthesis of Solids: To synthesize solid **S1**, 25 circular NAA supports (2 mm) were immersed in a rhodamine B solution in CH_3CN (1.57 mM, 6 mg, 8 mL) and stirred for 24 h to load the pores. Surface functionalization was achieved by adding (3-triethoxysilyl) propylisocyanate (328 µL, 1.32 mmol) and stirring the mixture for 5 h and 30 min. The material was then allowed to dry at room temperature overnight. To obtain solid **S2**, **S1** was immersed in a solution containing the appropriate nucleotide sequence (**O1**) in rhodamine B (262.5 µg, 1.57 mM, 350 µL) and TEA (2 µL) in CH_3CN. Solid **S3** was then obtained by immersing the same solids in a hybridization buffer (pH 7.5, 20 mM TRIS-HCl, 37.5 mM $MgCl_2$) with the DNA aptamer (**O2**). To optimize the capping conditions and improve performance, 50 µL of **O1** (10 µM) and 10 µL of **O2** (100 µM) were used in a final volume of 125 µL of hybridization buffer, which was agitated at 25 °C for 120 min. The remaining oligonucleotide and rhodamine B were then removed through several washes with a hybridization buffer.

Cargo Quantification: To determine the capacity of solid **S3** to load rhodamine B, two independent supports were immersed in 1 mL of

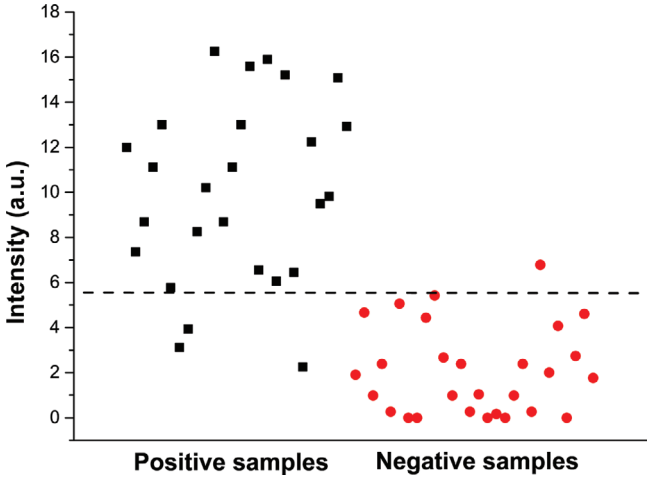

Figure 9. Measurement of dye release in presence of human nasopharyngeal samples. The scatter plot represents how levels are lower in negative samples ($n = 28$) (red dots) than in positive samples ($n = 26$) (black dots) establishing a discrimination limit in 5.6 fluorescence units.

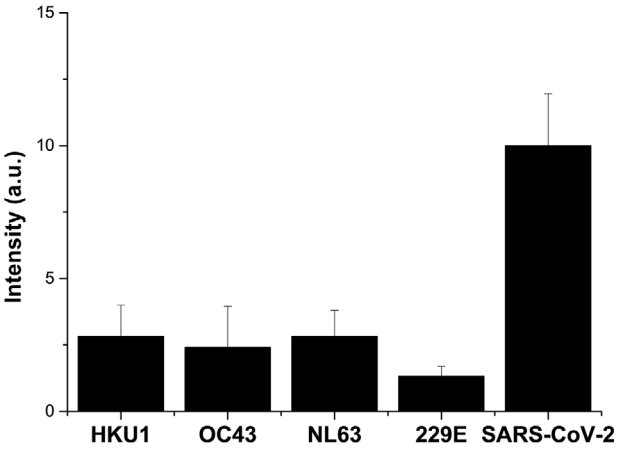

Figure 10. Rhodamine B release from probe **S3** in presence of samples infected with coronaviruses HKU1, OC43, NL63, 229E and a positive control of a nasopharyngeal sample infected with SARS-CoV-2 virus.

the hybridization buffer. One support was agitated at 25 °C for 60 min, while the other was stirred at 90 °C for 60 min to induce the release of cargo from the pores. The amount of fluorophore released was measured at 575 nm (λ_{exc} = 555 nm) using a calibration curve with different concentrations of rhodamine B. The experiment was repeated three times.

Virus Obtention: To generate the replication-competent vesicular stomatitis virus carrying the S protein of the Wuhan SARS-CoV-2 strain, we replaced the G gene in a plasmid encoding the antigenome of **VSV** with an additional GFP transcriptional unit[30] with the Wuhan spike sequence lacking the C-terminal 21 amino acids to facilitate virus production. The virus was then rescued as previously described[30] but using induced BHK-G43 cells which express the G protein of **VSV**.[31] The virus was then amplified for 1 passage on Vero cells. Replication incompetent **VSV** carrying different S proteins were produced as previously described.[32] The genotype of the S proteins relative to the Wuhan S sequences were: Alpha, mutations H69Del, V70Del, Y144Del, T716I, N501Y, D614G, P681H, A570D, S982A, and D1118H; Beta, mutations D80A, E484K, L242Del, A243Del, L241Del, N501Y, D614G, and A701V; Gamma, mutations L18F, D614G, T20N, P26S, R190S, D138Y, E484K, N501Y, K417T, H655Y, T1027I and V1176F; and Delta, mutations T19R, F157Del, R158Del, L452R, T478K, D614G, P681R, and D950N. All viruses were purified by centrifugation at 50,000g for 4 h and resuspended in DMEM All viruses were maintained in the same media at –80 °C.

Detection Protocol: The ability of the materials to detect spike protein was evaluated by measuring the fluorescence of rhodamine B diffused from the inner mesoporous structure in the presence and absence of the protein. To do this, two independent supports of material **S3** were each immersed in 900 µL of hybridization buffer. 100 µL of purified spike protein (1 ng µL^{-1}, Sinobiological, Beijing, China) was added to one support in each pair of **S3** solids, while the other received 100 µL of hybridization buffer. Aliquots were collected periodically while all solutions were stirred at 25 °C. The released rhodamine B was detected by fluorescence spectroscopy at 575 nm (λ_{exc} = 555 nm) and the experiment was repeated three times. In a subsequent step, a similar release assay was performed using 100 µL of **VSV-S** (2.5×10^5 PFU mL^{-1}) added to one support of **S3**, with all solutions stirred at 25 °C.

Quantification Curve of SARS-CoV-2 Spike Protein Recognition: The response of solid **S3** to various concentrations of **VSV** expressing the coronavirus spike protein on its surface was investigated. To do this, eleven independent samples of **S3** were each immersed in a solution containing 100 µL of different dilutions of **VSV-S** (ranging from 10^4 to 5×10^6 PFU mL^{-1}) and the volume was completed with 1 mL of hybridization buffer (resulting in a 1:10 dilution of the virus concentrations). The solutions were stirred at 25 °C and the released rhodamine B was determined at 575 nm (λ_{exc} = 555 nm) after 60 min. The same experiment was repeated using 900 µL of competitive media (a nasopharyngeal sample from a patient).

Selectivity: In order to evaluate the selectivity of the system, a series of dye release experiments were performed using independent samples of material **S3** and known concentrations of various drugs. The drugs tested included levothyroxine (0.025 mg mL^{-1}), acetylsalicylic acid (0.05 mg mL^{-1}), salbutamol (0.1 mg mL^{-1}), paracetamol (0.1 mg mL^{-1}), enoxaparin (0.1 mg mL^{-1}), and tiotropium (0.05 mg mL^{-1}). In addition, it was used 100 µL of SARS-CoV-2 spike protein (1 ng µL^{-1}) as a positive control, and a negative control was included in the form of 100 µL of hybridization buffer.

To conduct the experiments, the samples of material **S3** were immersed in a solution containing the test compounds, and the mixture was completed to a final volume of 1 mL with hybridization buffer. The solutions were stirred for 60 min at 25 °C, after which fluorescence measurements were taken to quantify the amount of rhodamine B released (λ_{exc} = 555 nm, λ_{em} = 585 nm). The experiments were repeated multiple times to ensure accuracy.

Validation in Competitive Media: To evaluate the ability of the sensing material **S3** to detect different concentrations of **VSV-V** in a more realistic environment, virus samples were first diluted to a concentration of 2.5×10^4 PFU mL^{-1}. Subsequently, human nasopharyngeal samples were collected from four healthy donors using a swab and stored in 5 mL of hybridization buffer. The samples were then artificially inoculated with the prepared virus concentration. Finally, four independent samples of **S3** were immersed in 100 µL of each nasopharyngeal sample plus 900 µL of hybridization buffer. After stirring the mixture at 25 °C for 60 min, the fluorescence emission at 575 nm (λ_{exc} = 555 nm) was measured to determine the amount of rhodamine B delivered.

Study of the System Behavior with Different **VSV-S** *Variants*: To assess the responsiveness of the system to the constant changing of SARS-CoV-2 that have naturally occurred during all the pandemic, different virus variants were tested with independent **S3** supports. Thus, **VSV** carrying the different S protein variants Alpha, Beta, Gamma, and Delta, which are the most spread in European countries until December 2021, were used. All the different four variants were diluted to a concentration of $2{,}5 \times 10^4$ PFUmL^{-1}, meanwhile the control essay was performed containing no virus. All viruses were first diluted in TRIS media and then 100 µL of each one was added to 900 µL of competitive media (nasopharyngeal sample) containing a final volume of 1 mL in each microtube. Released rhodamine B after 60 min was measured by fluorescence as in previous experiments (λ_{exc} = 555 nm). Processing of the data collected was carried out prior to its representation. This treatment consisted of subtracting the control value from all the intensity values of the different groups studied. Subsequently, these values were relativized to a scale of 0–10, with 10 being the highest fluorescence value and 0 the lowest.

Analytical Performance in Real Nasopharyngeal Samples from Suspected COVID-19 Patients: In the final step, the nanodevice behavior in nasopharyngeal samples was tested and its performance was compared with the reference method (RT-qPCR). Tested samples were taken from patients suspected of presenting a SARS-CoV-2 infection at the Hospital Universitari i Politècnic La Fe in Valencia following the approval of the pertinent committees. Anonymization procedures were applied in order to protect patient data. Two different nasopharyngeal samples were obtained from each patient. One sample was collected using a multi-collect specimen collection kit tube (Abbott Lab S.A, Spain) or a viral transport medium (Vircell S.L., Spain) and was used for the analysis using the reference method. Another sample was collected also using clinical swabs but transported in TRIS buffer and was used to study the performance of the developed nanodevice **S3**.

Nasopharyngeal swabs for RT-qPCR were inactivated with Nuclisens Lysis Buffer (bioMerieux S.A., Spain). RNA extraction was performed by the in QiaSymphony SP/AS instrument automatized method (Quiagen Iberia S.L., Spain) with extraction protocol complex DSP Virus/Pathogen Kit (Quiagen Iberia S.L., Spain), using a 200 µL sample volume and eluting in a volume of 60 µL. The detection of COVID-19 (N gene) and other SARS-related coronaviruses (E gene) was performed using real-time reverse transcription and amplification of nucleic acids in a single step with the C1000 Touch Thermal Cycler (Bio-Rad Lab S.A. Spain) and SARS-COV-2 Realtime PCR Kit (Vircell S.L., Spain). The assay also included endogenous human RNAse P as a control. Samples collected for testing with **S3** were analyzed in duplicate. For this, individual samples of **S3** were placed in 995 µL of TRIS and 5 µL of nasopharyngeal sample (0.5%) was added to each, resulting in a final volume of 1 mL per vial. The released rhodamine B was then measured by fluorescence after 60 min of incubation (λ_{exc} = 555 nm), as previously done in other experiments.

Supporting Information

Supporting Information is available from the Wiley Online Library or from the author.

Acknowledgements

This study was supported by the Spanish Government (projects PID2021-126304OB-C41, and PID2021-122875OB-100 (MCUI/AEI/FEDER, UE)), the Generalitat Valenciana (project no.2 RD 180/2020,

CIPROM/2021/007), Supera COVID-19 Fund (DIACOVID project), the Universitat Politècnica de València–Instituto de Investigación Sanitaria La Fe (IIS-LaFe) (SARS-COV-2-SEEKER and VISION-COV projects), and by the European Commission –NextGenerationEU, through CSIC's Global Health Platform (PTI Salud Global) to Ron Geller. The project leading to this application has received funding from the European Union's Horizon EUROPE research and innovation programme under grant agreement No 101093042. Isabel Caballos thanks the Instituto de Salud Carlos III for her predoctoral fellowship (IFI21/00008). Alba López-Palacios thanks the Ministerio de Universidades for her predoctoral grant (FPU20/05297). Ron Geller holds a Ramon y Cajal fellowship from the Spanish Ministerio de Economía y Competitividad (RYC-2015-17517). Figure 1 done with BioRender.com. The use of samples from human subjects was approved by the Medicaments Research Ethics Commmittee, CEIm of Hospital Universitari i Politècnic La Fe (no. 2021-012-1). Informed written consent was obtained from all participants or next of kin prior to the research.

Conflict of Interest

The authors declare no conflict of interest.

Data Availability Statement

The data that support the findings of this study are available from the corresponding author upon reasonable request.

Keywords

aptamers, gated materials, optical sensors, nanomaterials, SARS-CoV-2

Received: November 10, 2022
Revised: December 25, 2022
Published online: March 20, 2023

[1] Johns Hopkins University & Medicine, "NEW COVID-19 Cases Worldwide", https://coronavirus.jhu.edu/map.html (accessed: November 2022).
[2] C. M. Das, Y. Guo, G. Yang, L. Kang, G. Xu, H.-P. Ho, K.-T. Yong, *Adv. Theory Simul.* **2020**, *3*, 2000185.
[3] T. Ji, Z. Liu, G. Wang, X. Guo, S. Akbar khan, C. Lai, H. Chen, S. Huang, S. Xia, B. Chen, Y. Chen, Q. Zhou, *Biosens. Bioelectron.* **2020**, *166*, 112455.
[4] S. A. Hashemi, N. G. Golab Behbahan, S. Bahrani, S. M. Mousavi, A. Gholami, S. Ramakrishna, M. Firoozsani, M. Moghadami, K. B. Lankarani, N. Omidifar, *Biosens. Bioelectron.* **2021**, *171*, 112731.
[5] G. Guglielmi, *Nature* **2020**, *583*, 506.
[6] L. Huang, L. Ding, J. Zhou, S. Chen, F. Chen, C. Zhao, J. Xu, W. Hu, J. Ji, H. Xu, H. Xu, G. L. Liu, *Biosens. Bioelectron.* **2021**, *171*, 112685.
[7] C. S. Pavia, M. M. Plummer, *J. Microbiol. Immunol. Infect.* **2021**, *54*, 776.
[8] R. Liu, L. He, Y. Hu, Z. Luo, J. Zhang, *Chem. Sci.* **2020**, *11*, 12157.
[9] N. Bhalla, Y. Pan, Z. Yang, A. F. Payam, *ACS Nano* **2020**, *14*, 7783.
[10] L. M. Bellan, D. Wu, R. S. Langer, *WileyInterdiscip. Wiley Interdiscip Rev. Nanomed. Nanobiotechnol.* **2011**, *3*, 229.
[11] À. Ribes, E. Aznar, A. Bernardos, M. D. Marcos, P. Amorós, R. Martínez-Máñez, F. Sancenón, *Chem., - Eur. J.* **2017**, *23*, 8581.
[12] À. Ribes, E. Xifré-Pérez, E. Aznar, F. Sancenón, T. Pardo, L. F. Marsal, R. Martínez-Máñez, *Sci. Rep.* **2016**, *6*, 38649.
[13] L. Pla, A. Aviñó, R. Eritja, A. Ruiz-Gaitán, J. Pemán, V. Friaza, E. J. Calderón, E. Aznar, R. Martínez-Máñez, S. Santiago-Felipe, *J. Fungi* **2020**, *6*, 292.
[14] A. Ahmad, J. E. Spencer, S. R. Lockhart, S. Singleton, D. J. Petway, D. A. Bagarozzi, O. T. Herzegh, *Mycoses* **2019**, *62*, 513.
[15] L. Pla, S. Santiago-Felipe, M. Á. Tormo-Mas, J. Pemán, F. Sancenón, E. Aznar, R. Martínez-Máñez, *Sens. Actuators, B* **2020**, *320*, 128281.
[16] L. Pla, S. Santiago-Felipe, M. Á. Tormo-Mas, A. Ruiz-Gaitán, J. Pemán, E. Valentín, F. Sancenón, E. Aznar, R. Martínez-Máñez, *Emerg. Microbes Infect.* **2021**, *10*, 407.
[17] A. B. Iliuk, L. Hu, W. A. Tao, *Anal. Chem.* **2011**, *83*, 4440.
[18] Y. Seok Kim, N. H. Ahmad Raston, M. Bock Gu, *Biosens. Bioelectron.* **2016**, *76*, 2.
[19] R. Kumar, S. Nagpal, S. Kaushik, S. Mendiratta, *Virusdisease* **2020**, *31*, 97.
[20] T. Farrow, S. Laumier, S. Hall, I. Sandall, H. Van Zalinge, *IEEE Sens. J.* **2020**, *12*, 347.
[21] M. Amouzadeh Tabrizi, L. Nazari, P. Acedo, *Sens. Actuators. B* **2021**, *345*, 130377.
[22] A. Pramanik, Y. Gao, S. Patibandla, D. Mitra, M. G. McCandless, L. A. Fassero, K. Gates, R. Tandon, P. C. Ray, *J. Phys. Chem. Lett.* **2021**, *12*, 2166.
[23] Y. Song, J. Song, X. Wei, M. Huang, M. Sun, L. Zhu, B. Lin, H. Shen, Z. Zhu, C. Yang, *Anal. Chem.* **2020**, *92*, 9895.
[24] J. K. Millet, T. Tang, L. Nathan, J. A. Jaimes, H. L. Hsu, S. Daniel, G. R. Whittaker, *J. Vis. Exp.* **2019**, *145*, 59010.
[25] J. B. Case, P. W. Rothlauf, R. E. Chen, Z. Liu, H. Zhao, A. S. Kim, L. M. Bloyet, Q. Zeng, S. Tahan, L. Droit, M. X. G. Ilagan, M. A. Tartell, G. Amarasinghe, J. P. Henderson, S. Miersch, M. Ustav, S. Sidhu, H. W. Virgin, D. Wang, S. Ding, D. Corti, E. S. Theel, D. H. Fremont, M. S. Diamond, S. P. J. Whelan, *Cell Host Microbe* **2020**, *28*, 475.
[26] S. Pfefferle, S. Reucher, D. Nörz, M. Lütgehetmann, *Euro Surveill* **2020**.
[27] G. C. Mak, P. K. Cheng, S. S. Lau, K. K. Wong, C. S. Lau, E. T. Lam, R. C. Chan, D. N. Tsang, *J. Clin. Virol.* **2020**, *129*, 104500.
[28] R. Wölfel, V. M. Corman, W. Guggemos, M. Seilmaier, S. Zange, M. A. Müller, D. Niemeyer, T. C. Jones, P. Vollmar, C. Rothe, C. Drosten, C. Wendtner, *Nature* **2020**, *581*, 465.
[29] À. Ribes, S. Santiago-Felipe, A. Bernardos, M. D. Marcos, T. Pardo, F. Sancenón, R. Martínez-Máñez, E. Aznar, *ChemistryOpen* **2017**, *6*, 653.
[30] I. Andreu-Moreno, R. Sanjuán, *mBio* **2020**, *11*, e02156.
[31] A. Hanika, B. Larisch, E. Steinmann, C. Schwegmann-Weßels, G. Herrler, G. Zimmer, *J. Gen. Virol.* **2005**, *86*, 1455.
[32] R. Gozalbo-Rovira, E. Gimenez, V. Latorre, C. Francés-Gómez, E. Albert, J. Buesa, A. Marina, M. L. Blasco, J. Signes-Costa, J. Rodríguez-Díaz, R. Geller, D. Navarro, *J. Clin. Virol.* **2020**, *131*, 104611.